Kinetics and mechanism of hydroxyl radical formation studied via electron spin resonance for photocatalytic nanocrystalline titania: Effect of particle size distribution, concentration, and agglomeration

Sasiporn Sroiraya[a]**, Wannapong Triampo**[b,c,e]**, Noppawan Phumala Morales**[d] **and Darapond Triampo**[a,c,e,]*
[a]*Department of Chemistry (R3/1)*
[b]*R&D Group of Biological and Environmental Physics (BIOPHYSICS), Department of Physics*
[c]*Center of Excellence for Vectors and Vector-Borne Diseases*
[d]*Department of Pharmacology in the Faculty of Science*
[e]*Institute for Innovation and Development of Learning Process, Mahidol University, Salaya Campus, Phuttamonthon Sai 4 Rd.,
Nakhon Pathom 73170, Thailand*

A photocatalytic process was carried out with two types of TiO_2: commercial (C-TiO_2) and in-house synthesized (S-TiO_2). Parameters, such as, initial particle concentration and the nanoparticle (NPs) agglomerations effect on hydroxyl radical ($\bullet OH$) concentration were investigated using electron spin resonance (ESR) spectroscopy with a spin trapping technique. The experimental results demonstrate that generation of $\bullet OH$ and DMPO/$\bullet OH$ (5,5-dimethyl-1-pyrolline-N-oxide/hydroxyl radical) adduct formation is controlled by a shorter time-scale of the chemical reaction on particle surfaces and longer time-scale particle agglomerations in the bulk dynamics. It was found that S-TiO_2 has a smaller particle size than C-TiO_2 NPs. As a consequence, S-TiO_2 NPs yield a higher concentration of $\bullet OH$ compared to that of C-TiO_2 NPs of the same concentration. These findings reveal an agreement between the ESR signals, agglomeration size analysis, and transmission electron microscopy (TEM) data. Detail explanations are presented mainly on the drive of dynamic time scales and the limitation of the number of NPs governed by their associated distributions. With the kinetic studies, we propose the mechanism for the generation of $\bullet OH$ via a study of ESR DMPO/$\bullet OH$ spin trap technique. The mechanism accounts for the active surface area as the agglomeration process occurred throughout the suspension and the possibility of DMPO/$\bullet OH$ recombination as the surface of TiO_2 became dense with DMPO/$\bullet OH$ adduct.

Key words: Nanoparticles, titanium dioxide (TiO_2), agglomerate, photocatalysis, hydroxyl radical, ESR.

Introduction

Titanium dioxide (TiO_2 or titania) powders and films (coatings) have been widely researched in recent years. The photocatalytic processes on TiO_2 can be initiated by solar radiation. TiO_2 efficiency to decontaminate water and air depends on many factors: such as, type, source, and concentration of the impurity to be removed, applied photocatalytic technique, and source of light, etc. For the application in water and air purification [1-2], its photocatalysis has drawn more and more attention from scientists and engineers [3-7]. Power generation and hydrogen production from solar energy is also a potential application field [8-10]. Although much effort has been made, the mechanism of TiO_2 photocatalysis is not well understood up to now [11].

Photocatalytic events occur after ultraviolet light (UV) with a wavelength of less than 385 nm is illuminated on TiO_2 (band-gap energy of anatase, 3.2 eV, brookite

3.4 eV, and rutile, 3.0 eV). It subsequently causes the formation of electron/hole pairs (excitons) on the surface or near it [12]. Following electron/hole separation, the two charge carriers quickly migrate to the surface through diffusion and drift, in competition with a multitude of trapping and recombination of events in the bulk lattice. It is known that an electron-hole pair, after being generated, can diffuse and recombine in the volume of titania particles. It was suggested that such a pair can also be localized at the surface. Surface-localized electrons may result in the formation of an $\bullet O_2^-$ anion, and ultimately, in the formation of hydrogen peroxide [13]. Since the surface-localized hole and electron produce different active species, they lead to totally different reaction pathways. Thus, information on the location of the electron-hole pair is crucial in understanding the mechanisms of photocatalytic processes on TiO_2 surfaces. At the surface, these carriers are poised to initiate redox chemistry with suitable pre-adsorbed acceptor and donor molecules in competition with recombination events to yield radiative and non-radiative emissions, and/or trapping of the charge carriers into shallow traps at lattice sites. Thus, on absorption of UV light, titania particles yield several

*Corresponding author:
Tel : +662-441-9817
Fax: +662-889-2337
E-mail: scdar@mahidol.ac.th

different species especially reactive oxygen species (ROS) including dominant hydrogen peroxide (H_2O_2), super oxide radical anions ($\bullet O_2^-$) and hydroxyl radicals ($\bullet OH$) [11,14].

In this study, special attention is paid to the $\bullet OH$ species. These $\bullet OH$ species are mostly (almost only) on the TiO_2 surface because of the very short-lived time scale (in nanoseconds) [12], compared to the diffusion time scale. However, there is a possibility of $\bullet OH$ forming and desorbing from the surface as well. All together, most studies proposed that the bactericidal effect of photocatalysis with TiO_2 could be due to the generation of ROS. And the majority of these studies concluded that $\bullet OH$ was the main cause of the bactericidal effect of photocatalysis [15-16].

The biological and environmental applications of TiO_2, using TiO_2 nanoparticles in the suspension or colloid form [17-20] may be one of the best-known applications aside from in thin film form [21-22]. However, there remain some not well understood issues regarding, 1) what mechanisms the radicals generated by TiO_2 photo catalysis damage or kill cells, 2) how the particle agglomerations effect [23-25] the photocatalytic efficacy to generate radicals, and 3) how much effect the interactions between those radicals both of the same and different radical species has on the photocatalytic efficacy. To answer or at least provide *some insight* as to what may contribute to some of the answers of the above mentioned questions is one of the aims of this study.

Electron spin resonance (ESR) spectroscopy is used to study the kinetics and mechanism of the interaction between $\bullet OH$ and the spin trapping agent DMPO in connection to DMPO/$\bullet OH$ adduct production and ESR signals. Because $\bullet OH$ are short-lived, the spin trapping technique is employed to allow us to detect the amount of $\bullet OH$ with the use of the spin trapping agent DMPO. The effects of particle agglomerations and other possible short- and long-time scale perturbations are also considered. The observed ESR signal spectra and their non-linear effects depend on the applied microwave power, frequency, and amplitude of the steady magnetic field modulation or the magnetic field sweep time. All these parameters are to be controlled in this study.

The scope of this study is to detect $\bullet OH$ in irradiated TiO_2 using an ESR spin trapping technique. Various concentrations of TiO_2-NPs with different exposure times to UV-A irradiation are studied. Production of $\bullet OH$ from in-house synthesized TiO_2-NPs (S-TiO_2) is investigated in comparison to commercial TiO_2-NPs (C- TiO_2). The mechanism of the dynamics of photocatalytic DMPO/$\bullet OH$ in correlation to ESR signals under the conditions studied, especially, taking into account nano- particle agglomeration is our ultimate goal.

Materials and methods

Chemical reagents

Titanium dioxide (commercial TiO_2, C-TiO_2, 99.9% pure nanopowder), a standard solution of H-TEMPO (4-hydroxyl-2,2,6,6-tetramethyl-piperidinyloxyl radical), and a spin trapping reagent DMPO (5,5-dimethyl-1-pyrolline- N-oxide) were purchased from Aldrich. Activated charcoal was purchased from Ajax Finechem. Titanium (IV) isopropoxide ($Ti(OC_3H_7)_4$) (short form TTIP) and 2-propanol (($CH_3)_2CHOH$, 99.8%) were purchased from Fluka. Hydrochloric acid (HCl, 35.4%) was purchased from Anala R. All reagents were of analytical grade.

In-house synthesis TiO_2 nanoparticles (S-TiO_2)

A volume (1 ml) of water was premixed with 50 ml of 2-propanol. Then a mixture of 6 ml TTIP and 25 ml of 2-propanol was added to the premix and kept sonicated for 2 hours. The solution was later dried at room temperature to evaporate the 2-propanol. The thin film obtained was manually ground for 10 minutes to obtain fine powder. The sample was calcinated at 550°C for 2 hours to obtain S-TiO_2 [26-29].

X-ray diffraction (XRD) and transmission electron microscopy (TEM) analysis

Powder X-ray diffraction (XRD, Bruker D8 Advance) was used to identify the crystal phases of S-TiO_2 in comparison to C-TiO_2. XRD settings were performed with a monochromatic Cu-K_α (40 kv, 30 mA) source, step size of 0.037311°, and a step time 1 s/step.

TEM micrographs were taken using a Tecnai G2 Sphera operating at a voltage of 80 kV. All samples were prepared by dropping the suspension from the particle size analyzer onto a holey-carbon TEM grid and dried at room temperature. TEM micrographs compared the particle agglomerate size. From TEM analysis, ensemble average of particle sizes over at least 10 configurations, the average particle size was determined.

Study of UV-irradiation time on the production of $\bullet OH$ radical for both C-TiO_2 and S-TiO_2 nanoparticles

The production of $\bullet OH$ radical was determined by ESR using DMPO as a spin trapping agent. DMPO was purified prior to use by adding activated charcoal into the DMPO solution subsequent to centrifugation at 12000 rpm for 20 minutes. Concentrations (0, 5, 10, 20, 30, 40, 50, and 70 ppm) of both C-TiO_2 and S-TiO_2 nanoparticles were prepared and 10 µl of 1.4M of DMPO was added. The mixtures were transferred to a capillary tube and fitted into the cavity of the ESR spectroscopmeter. Studied samples were directly irradiated in the microwave cavity with focused light from a UV mercury lamp, HBO 50 W/AC (ER 202 UV version 1.0/ KAMI, 300 < wavelength < 385). ESR spectra were recorded at various times after UV exposures. ESR measurements were performed by a standard X-band electron spin resonance spectrometer (E 500, Bruker, USA equipped with ELEXSYS Super High Sensitivity Probehead cavity). The ESR spectrometer settings were as follows: magnetic field 3355 ± 50 Gauss, modulation frequency 100 KHz, modulation amplitude 1.25 Gauss, microwave frequency 9.8 GHz, microwave

power 10.2 mW, sweep time 41.94 ms and time constant, 5.12 ms.

Quantitative analysis of ESR spectrum

A typical $1 : 2 : 2 : 1$ quartet-line ESR spectra of DMPO/●OH adduct can be observed in Fig. 1 [30]. UV irradiation of the aqueous suspension of TiO_2 containing DMPO gives the ESR spectrum, with g = 2.0060 and coupling constant $a_N = a_H = 14.9$ Gauss. This spectrum has been previously identified by Harbour and co-workers [31-32] by UV irradiation of H_2O_2 solution in the presence of DMPO.

To quantify DMPO/●OH adduct, integration of the ESR signal area was performed and the concentration of ●OH was determined from the standard spin concentration curve of H-TEMPO.

Agglomeration study with particle-size analyzer

Two hundred milligrams of TiO_2 was dispersed in 50 ml of deionized water. Agglomerates of TiO_2 were dispersed using an ultrasonic homogenizer (Hydro MU, 40 kHz) equipped on a particle-size analyzer (MASTERSIZER 2000, Malvern Instruments). The experimental setup used a homogenizer rotor speed of 2000 rpm. The measurements were performed with absorbance ranging

from 5 to 10%. The measurement were made by averaging at least three repeats. The sonication amplitude was fixed at 20 micrometer for 10 minutes, then turned-off. Measurements recorded with the particle-size analyzer to study the agglomeration process over time were made after the ultrasonic homogenizer was turned-off. A reading taken at the time the ultrasound was turned-off is marked as 0 minute, and then followed by 2, 3, 5, 7, 8, and 10 minutes.

Results and discussion

Crystal phases of S-TiO₂ in comparison to C-TiO₂

XRD patterns shown in Fig. 2 indicate that anatase is the major phase for both $S-TiO_2$ and $C-TiO_2$. $S-TiO_2$ has ~8 % of brookite phase formed (Fig. 2a). While the ratio of anatase to rutile for $C-TiO_2$ is ~2 : 1 (Fig. 2b). A peak broadening effect is observed for $S-TiO_2$ as commonly observed in XRD patterns of nanocrystals.

### Particle-size analysis with transmission electron microscopy (TEM)

First, the ensemble particle sizing characterization was performed by TEM. Fig. 3 reveals the particle size configurations of both $C-TiO_2$ and $S-TiO_2$. It is evident that agglomeration did occur, consequently forming secondary, tertiary or larger agglomerate size. From the particle images obtained, ensemble averages of particle sizes over at least 10 configurations were performed. It was found that for $C-TiO_2$, the particle size ranged from 10-150 nm with the size average of 42±10 nm. This is within the size range specified by the manufacturer which is 20-60 nm and a surface area of about 20-25 m^2/g. The differences may be due to the sample preparation procedures and characterization techniques. However, these particle size distributions, obtained are on average are much larger than those of $S-TiO_2$ which were estimated
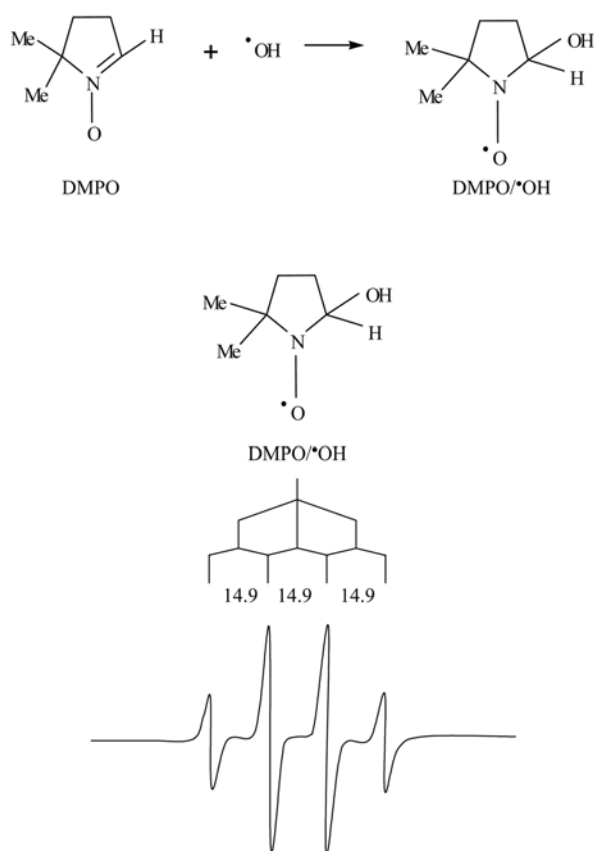
Fig. 1. Shows spin trap of ●OH radical with DMPO and DMPO/ ●OH ESR hyperfine splitting of 14.9 Gauss. This is characteristic of a DMPO adduct ($1 : 2 : 2 : 1$ quartet with hyperfine coupling of $a_N = a_H = 14.9$ Gauss) produced by spin trapping of a hydroxyl radical produced in a hydroxyl radical-generating system.
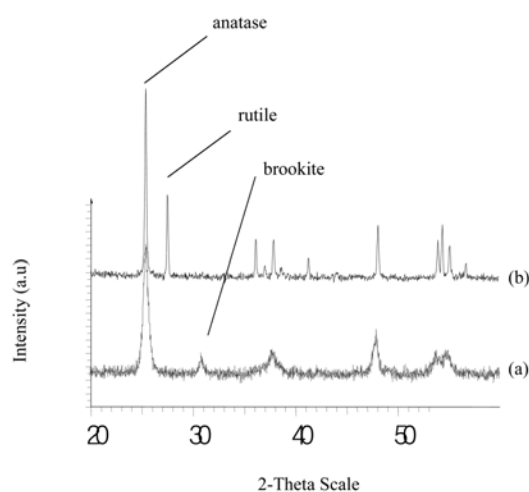
Fig. 2. Typical broad-scan XRD patterns within the 2θ range of 20-60° obtained from (a) $S-TiO_2$ after calcination at 550°C for 2 h and (b) $C-TiO_2$ from Aldrich.
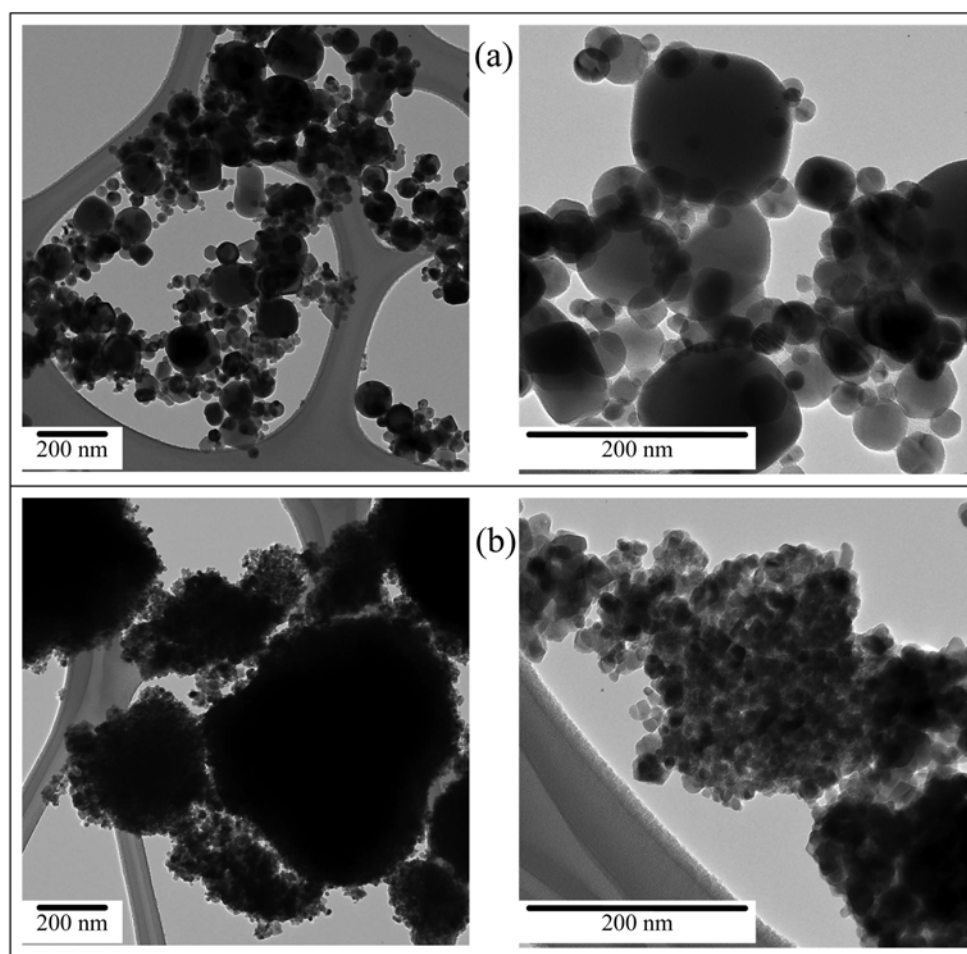
Fig. 3. TEM micrographs (a) of C-TiO$_2$ and (b) of S-TiO$_2$. Micrographs show a distinct particle size difference between commercial and synthesized TiO$_2$.

to range from 8-120 nm with the average of 15±4 nm and a surface area of 80-85 m^2/g. These data imply that the particle surface to volume ratio of S-TiO$_2$ is 4 times larger than that of C-TiO$_2$. It is important to note that the particle size distribution is typically time dependent and not stable due to agglomeration and precipitation effects [24] which are governed by the competition of the force fields such as the van der Waals attraction force, the electrostatic repulsive force, the Brownian diffusive drive, and the gravitational field. This directly results from the reaction–diffusion process of particles [33]. Typically, it may take an asymptotic long time for the suspension sample to reach a global equilibrium state resulting in a stable size distribution.

Hydroxyl radical analysis with electron spin resonance (ESR)

Fig. 4 represents sampled ESR spectra that correspond to different concentrations of •OH. Each ESR spectrum was integrated and the peak area is extracted to determine the concentration of •OH from the standard calibration curve using H-TEMPO (not shown). Without UV-irradiation (time = 0) or in the absence of TiO$_2$ (0 ppm) but with exposure to UV (up to 13 minutes), the ESR signal of

DMPO/ •OH adduct was not detected (as in Fig. 4a). This implies that •OH are mainly generated by the photocatalytic process of TiO$_2$ through electron-hole pair production interacting with H$_2$O rather than the photolytic process due to the UV photon interacting with the sample media. This is due to the relatively low dose of UV irradiation. From Fig. 4a to 4d, the data were taken from samples of C-TiO$_2$ with concentrations of 0, 5, 20 and 70 ppm, respectively. As expected, for these particular cases the •OH concentration rises from 0 to 2.00 ± 0.13 μM. This is consistent with the fact that the higher the surface area of the catalyst, the larger the reaction rate will be. In our case, this was indicated by the redox reaction on the particle surface.

Fig. 5a and 5b plots the time of UV-irradiation versus the concentration of •OH for the different concentrations of C-TiO$_2$ and S-TiO$_2$, respectively. This is to study the effects of TiO$_2$ concentration on the production of •OH. It was found that initially or at the time of 0 minute UV irradiation, TiO$_2$ does not generate •OH. For the relatively low TiO$_2$ concentrations (< 20 ppm), the concentration of DMPO/^{2}OH adducts increased in an irradiated-time period dependent manner. Each increased with relatively
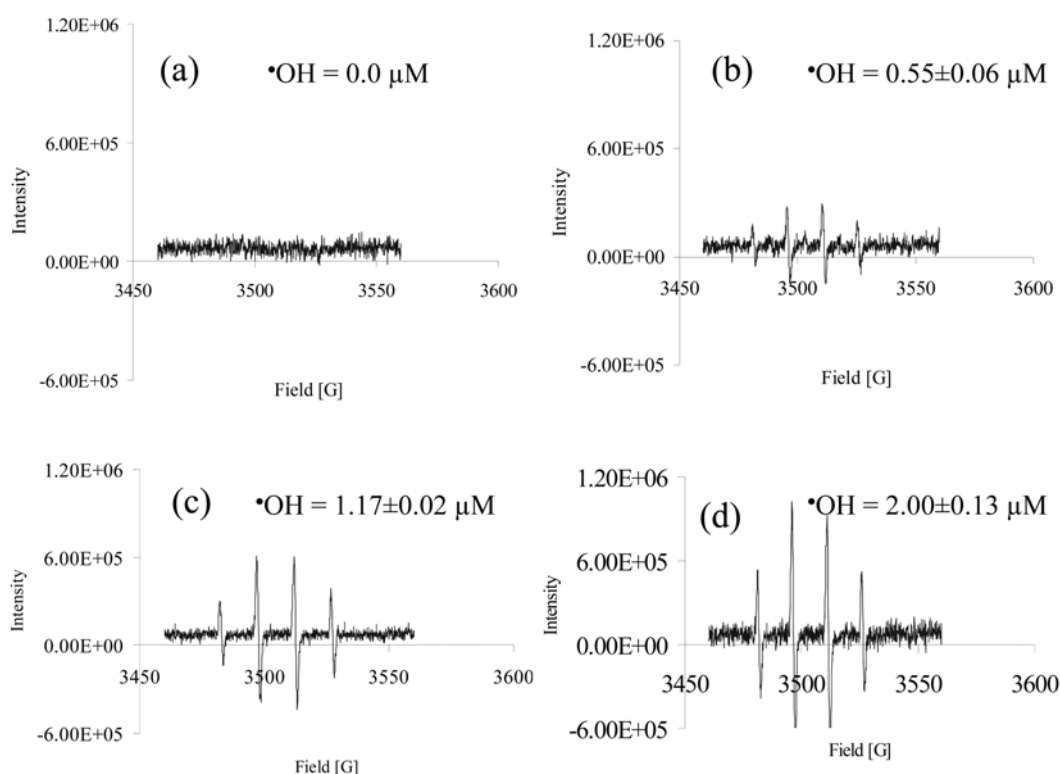
Fig. 4. ESR sampled spectra from different concentrations of C-TiO$_2$ suspension after 13 minutes of UV exposure corresponding to different concentrations of •OH.

high rates (with respect to the UV irradiation period or dose) early on called the *early regime* and reached a maximum after a few minutes. After that it crossed over to a *leveled-off regime* with very small change in the rate. In this leveled-off regime, if we look closely, the graphs appear to slightly decrease before they asymptotically reach a steady state.

For the relatively high TiO$_2$ concentrations (≥ 20 ppm), considering each graph after the high rate of increase of •OH in the early regime until it reaches the maximum •OH concentration which indicates the maximum time of UV irradiation for maximum •OH concentration, it then decreases but in a more pronounce manner than the previous case before it eventually reaches a steady state. These phenomena may be explained as follows. First, it is reasonable to say that the DMPO concentration used is in excess and saturated to make sure that the DMPO/•OH adduct to be produced is not limited by the amount of DMPO reagent. As seen in Fig. 4, the ESR signal data used to determine the amount of •OH are a direct indication of the amount of DMPO/•OH adduct. Hence, the increase (or decrease) in the graphs indicate the increase (or decrease) in the amount of •OH produced. Before being UV irradiated, the spin trap agent DMPO is in Brownian motion and is likely to be everywhere in the suspension system. After being UV irradiated, a photon is generated and reacts with TiO$_2$. DMPO is not changed by these photons (at least for these studied doses) [30]. Keep in mind that the intensity
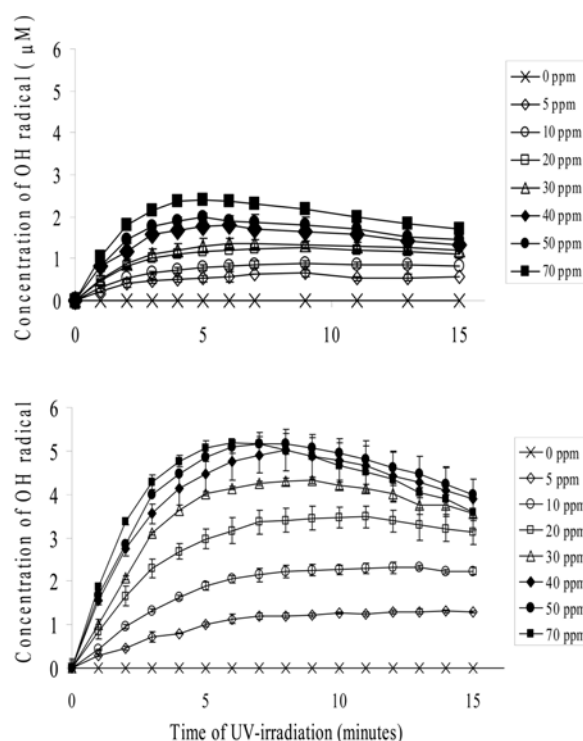
Fig. 5. Effect of UV-irradiation time of (a) C-TiO$_2$ and (b) S-TiO$_2$ suspension on •OH radical production.

and the frequency of this irradiating UV reflect the number of in-coming photons and the associated energy of each photon, respectively. With high enough light

energy ($\geq$ energy band gap of TiO_2), an electron-hole pair is created and results in a successful $\bullet$ OH production.

It virtually takes no time for $\bullet$ OH to react with DMPO to form a DMPO/$\bullet$OH adduct (which allows us to detect the $\bullet$ OH) and this occurs at a very high rate early on due to the high production rate of $\bullet$ OH. As time goes on, with a longer irradiation period, implying larger accumulation of $\bullet$ OH, this results in an increase in the amount of $\bullet$ OH, and consequently DMPO/$\bullet$OH adduct. For the case of a low TiO_2 concentration, since the DMPO/$\bullet$OH adduct is controlled and limited by the surface area of TiO_2 particles, the rate of increase is lower than those of high concentrations and exhibits just a slight change in the leveled-off regime. Indeed, as mentioned earlier, the amount of DMPO/$\bullet$OH adduct is slightly decreased before it finally reaches a steady state. The possible explanations are the agglomeration of TiO_2 particles and the recombination of two DMPO/$\bullet$OH that are close to each other that reduce the ESR signal. In addition, the spin trapped adduct can decompose by various mechanisms, such as, a dispro- portional reaction and hydrolysis.

To compare the previously mentioned results from C-TiO_2 with those from S-TiO_2, a similar plot of S-TiO_2 is shown in Fig. 5b. The overall qualitative features of both types are the same. Quantitatively, the surface area of S-TiO_2 is approximately 4 times that of C-TiO_2, for the same concentration of TiO_2 particles, but the concentration of $\bullet$ OH from S-TiO_2 is only twice as much that of C-TiO_2. A point also considered is that XRD results showed brookite in S-TiO_2 and rutile in C-TiO_2 (in Fig. 2). The difference in phases may have contributed to the amount of ^{2}OH being generated. However, from the studies by Ozawa *et. al.* [34] and Hurum *et. al.* [35], they reported an increase in photocatalytic activity with the coupling of both anatase-brookite and anatase-rutile compared to pure anatase. It could be predicted that anatase-brookite coupling would have lower photocatalytic activities than that of anatase-rutile coupling since the electronic structure of brookite is similar to that of anatase, therefore, brookite would not have extended the photoactivity of the mixed-phase in the same way rutile would [34-36]. Therefore, the higher concentration of $\bullet$ OH detected from S-TiO_2 must have been dominated by the particle size and agglomeration.

It is important to note that not only the maximum values of $\bullet$ OH are different, but also the associated UV-irradiation time or doses are shifted accordingly depending on the concentrations of TiO_2 particles for both C-TiO_2 and S-TiO_2. Fig. 6 plots the time to reach maximum $\bullet$ OH concentration for each concentration of TiO_2 with a logarithmic regression fitting. $y = -3.2043Ln(x) + 19.857$ and $R^2 = 0.9733$ for S-TiO_2 comparing to a fit of $y = -3.3788Ln(x) + 18.572$ and $R^2 = 0.9246$ for C-TiO_2. Logarithmic regression fitting gave the best fit among other: linear, power-law, and exponential regressions. It is to be noted that even though C-TiO_2 took less time to reach maximum $\bullet$ OH concentration,

but the maximum $\bullet$ OH concentration produced by C-TiO_2 is less than that of S-TiO_2. Whether there is a characteristic time scale or any universality concerning these phenomena is yet to be investigated.

Agglomeration evidence with particle-size analyzer

It is well known that a colloidal or suspension of particles tend to agglomerate as a result of energetic and entropic drives. These phenomena are governed by the short-range van der Waals interaction of particles. Because of the much larger time scale of bulk agglomeration compared to the DMPO/$\bullet$OH adduct formations time scale, this may be why this *lost* incident takes effect at a later time resulting in a decrease in the total surface area and the amount of DMPO/$\bullet$OH adduct (or ESR signal). An increase in the number of particles per given volume and constant collision of particles will cause particles to agglomerate and form more agglomerates. As agglomerated particles grow larger, the active surface area of TiO_2 is reduced, and therefore, less production of $\bullet$ OH with time. But for concentrations of 5 and 10 ppm, agglomeration phenomena are less due to the lesser number of particles per volume. The physical evidence of this agglomeration can also be verified by the TEM micrographs (Fig. 3).

Agglomerate size analysis with a particle size analyzer (Fig. 7) shows an increase in agglomerate size distribution with increasing time for both C-TiO_2 and S-TiO_2 suspension. Two peaks can be observed for all the times measured. From a time of 0-10 minutes, the peak ranging from 10-60 mm increases while the peak ranging from 0.2-3 mm decreases. This indicates a decrease in smaller agglomerates and an increase in larger agglo- merates. This result agrees well with our analysis of the ESR (Fig. 5) data. The term agglomerate size is used rather than particle size because as indicated from the TEM (Fig. 3) results, if the particle-size analyzer is to measure the primary particle size, we should observed peaks less than 100 nm.
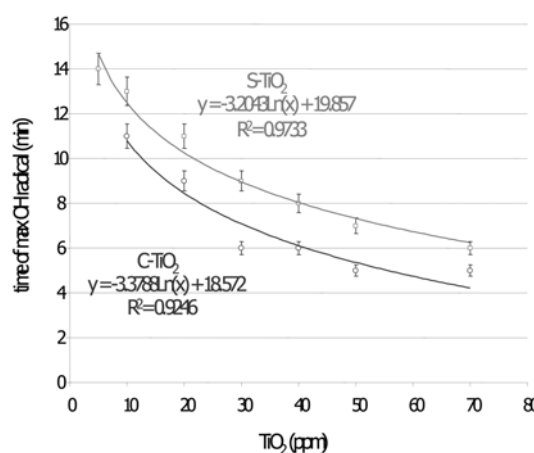
Fig. 6. Plots the time to reach maximum $\bullet$OH concentration for each concentration of TiO_2 with a logarithmic regression fitting. Logarithmic regression fitting gave the best fit among other: linear, power-law, and exponential regressions.
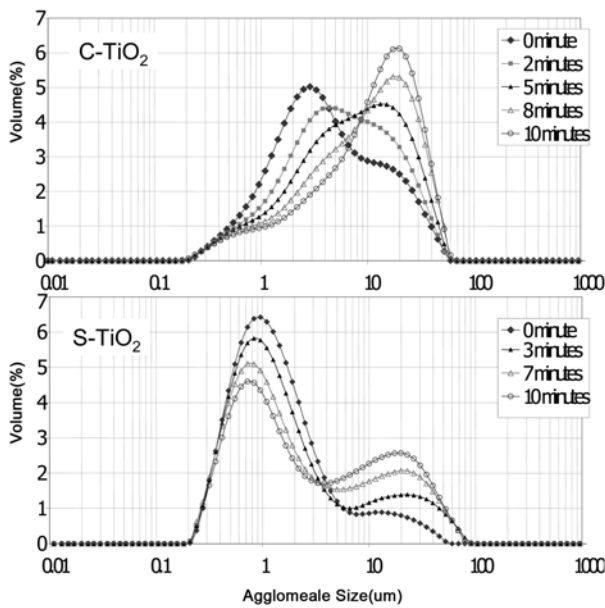
Fig. 7. Agglomerate size analysis with a particle size analyzer. Two peaks can be observed for all the times measured. From time of 0-10 minutes, the peak ranging from 10-60 μm increases while the peak ranging from 0.2-3 μm decreases.

But this is not the case, we can only detect the smallest agglomerate size to be 200 nm. Therefore, we believe it should be the agglomerate size that was being measured.

Besides the direct effect of particle agglomeration as mentioned earlier, the indirect effect or *agglomreation aftermath* due to particle precipitation may also be considered. The decrease in ESR signal is more evident with a sufficiently large particle size and when gravitational forces take effect. Another cause of the reduction of DMPO/ • OH signal is DMPO/ • OH recombination. It is known that DMPO/ • OH molecules that are nearby can react with each other [37]. Hence, this could be accounted for as another possible cause of the decline of ESR signal. However, this incident tends to occur when DMPO/ • OH adduct is densely populated on the surface which is likely to occur at a later time.

Finally, there are some issues that were left out early on to make the explanation less complicated. For example, the effect of the physically adsorbed O_2 molecules on the separation and stabilization of electron and hole centers on TiO_2 has been demonstrated previously [38-39]. Since our experiments did not focus on other
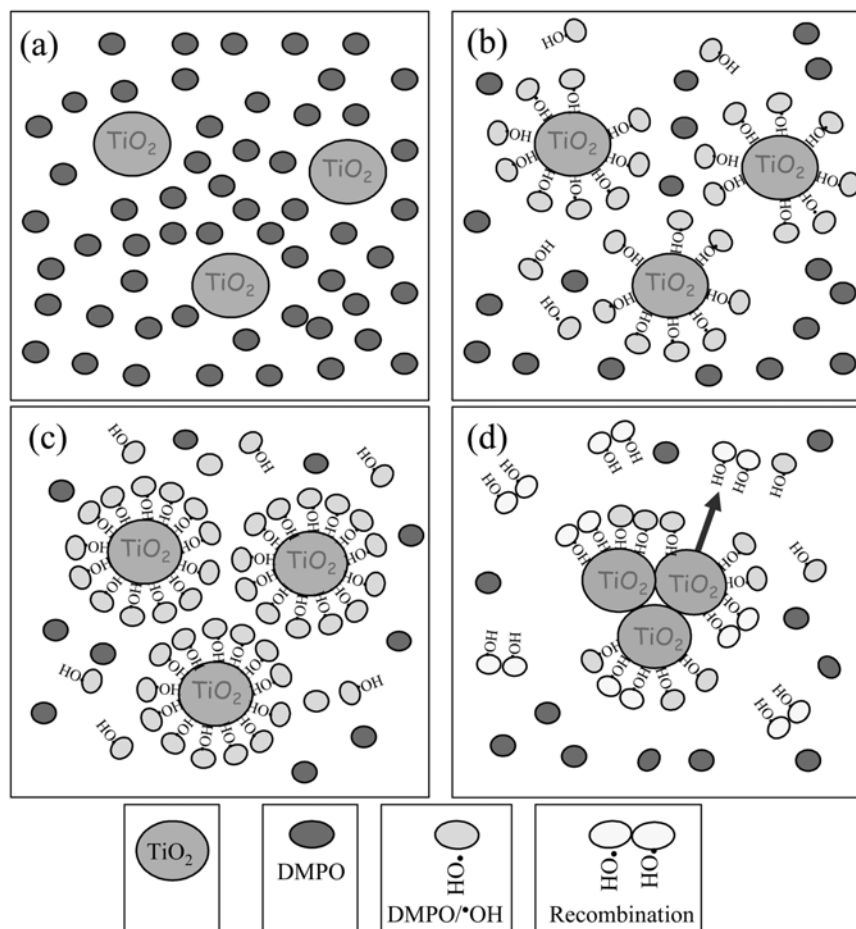
Fig. 8. Proposed mechanisms of •OH production on TiO_2 surface. (a) TiO_2 and DMPO at time 0 of irradiation; no production of •OH; no hyperfine splitting of DMPO/•OH. (b) increase in ESR signal as the suspension is initially irradiated; •OH is generated on TiO_2 surface; spin trapping of DMPO/•OH. (c) maximum ESR signal, as all •OH on TiO_2 surface are spin trapped by DMPO. (d) decrease in ESR signal as 2 DMPO/•OH that are in the vicinity of each other recombine.

radicals, the nature of the electron and hole centers formed upon irradiating TiO_2 and the nature of the states involved in the electron transfer are still open for discussion.

Mechanism of DMPO/ $\bullet$OH dynamics in TiO_2 photocatalysis with nanoparticle agglomerations

From the results discussed above, we propose the possible mechanism of DMPO/ $\bullet$OH adduct dynamics (quantified by the ESR results) of TiO_2 in photocatalysis as follows. Initially (Fig. 8a), at time of 0 minute UV irradiation, TiO_2 does not generate $\bullet$OH; therefore, no ESR signal of DMPO/$\bullet$OH adduct is detected. Right after the UV light is turned-on (Fig. 8b) and irradiated the TiO_2 suspension, $\bullet$OH is generated on the TiO_2 surface. The longer the irradiation time, the higher the amount of $\bullet$OH will be. Since $\bullet$OH is diffusive and very reactive, $\bullet$OH is spin trapped by DMPO yielding a longer half-life DMPO/ $\bullet$OH adduct, making it measurable by ESR. Whether the dynamics of the DMPO/ $\bullet$OH production may concern the diffusion of the DMPO to the TiO_2 surface or the coupling rate of DMPO/ $\bullet$OH adduct formation or the generation of $\bullet$OH to cover the entire TiO_2 surface is yet to be further investigated. Subsequently, after long enough time, the highest concentration level of DMPO/ $\bullet$OH adduct corresponding to maximum coverage of the $\bullet$OH on the TiO_2 surface that are spin trapped by DMPO is reached (maximum ESR signal is detected) as shown in Fig. 8c. Lastly Fig. 8d, among the competitions in the generation of new $\bullet$OH on the active surface; or agglomeration of particles in very complex ways (in analogy to polymerization); or the reactions between DMPO/ $\bullet$OH adduct and $\bullet$OH with other species, or even between themselves, etc. which could occur at a longer time scale, all of these factors would lead to the reduction of the active surface area for the generation of $\bullet$OH (or production rate) or even the number of DMPO/ $\bullet$OH adducts. When the concentration of a spin trapped adduct is high, the rate of disappearance is a second order, but the rate returns to first order when the concentration is low. To the best of our knowledge, this is the first time that the mechanism of the dynamics of DMPO/ $\bullet$OH adduct production associated with TiO_2 photocatalysis has been proposed.

Conclusions

We have demonstrated that TiO_2 irradiated with UV generates $\bullet$OH with DMPO as an ESR spin trapping agent. Considering various initial concentrations of TiO_2-NPs with different exposure times, production of $\bullet$OH from C-TiO_2 and S-TiO_2 NPs were investigated and compared. The key difference between this C-TiO_2 and S-TiO_2 was the particle/agglomerate size distribution which was analyzed by XRD, TEM, and A particle-size analyzer.

It was found that S-TiO_2 has smaller a particle size than C-TiO_2 NPs. The surface area of S-TiO_2 is four

times that of C-TiO_2 NPs. As a consequence, S-TiO_2 NPs yield higher concentrations of $\bullet$OH compared to those of C-TiO_2 NPs for the same concentration. This is believed mainly due to the agglomeration of NPs. These findings reveal an agreement between the ESR signals, TEM results, and agglomerate size analysis. Overall, the kinetics of each laboratory test is somewhat not straight forward as evidently seen from the existence of a maximum and decline to steady state at an asymptotically long time. Detailed explanations were presented mainly on the drive of dynamic time scales and the limitation of the number of NPs governed by their associated distributions. Also possible but very minor, this may be due to the non-linear cross feedback among ROS species.

With the kinetic studies, it allows us to propose a mechanism for the generation of $\bullet$OH via the study of the ESR spin trapping technique. The mechanism accounts for the active surface area as an agglomeration process occurring through the suspension and the possibility of DMPO/ $\bullet$OH recombination as the surface of TiO_2 becomes dense with DMPO/$\bullet$OH adduct. The mechanism can be used to support the antibacterial effect of TiO_2 photocatalysis that can be found in the literature. An investigation is underway to study anti-agglomeration effects on this system.

References

1. M. R., Hoffmann, S. T., Martin, W., Choi, and D. W. Bahnemann, Chem. Rev. 95 (1995) 69-96.
2. D. S. Ollis and H. A. Ekabi, in "Photocatalytic Purification and Treatment of Water and Air" (Elsevier, Amsterdam, 1993) p. 139-153.
3. J. R. Bolton, Sol. Energy 57 (1996) 37-50.
4. S. U. M. Khan and J. Akikusa, J. Phys. Chem. B 103 (1999) 7184-7189.
5. S. U. M. Khan and J. Akikusa, Int. J. Hydrogen Energy 27 (2002) 863-870.
6. O. Khaselev and J. A. Turner, Science 280 (1998) 425-427.
7. S. Licht, B. Wang, S. Mukerji, T. Soga, M. Umeno and H. Tributsch, J. Phys. Chem. 104 (2000) 8920-8924.
8. B. O'Regan and M. Gratzel, Nature 353 (1991) 737-740.
9. G. Rothenberger, P. Comte, and M. Grätzel, Sol. Energy Mater. Sol. Cells 58 (1999) 321-336.
10. G. Sauvé, M. E. Cass, S. J. Doig, I. Lauermann, K. Pomykal, and N. S. Lewis, J. Phys. Chem. B 104 (2000)

3488-3491.

11. A. L. Linsebigler, G. Q. Lu, and J. T. Yates, Chem Rev. 95 (1995) 735-758.

12. A. Sobczyñski and A. Dobosz, Polish Journal of Environmental Studies, 10 (2001) 195-205.

13. V. Shapovalov, E. V. Stefanovich, and T. N. Truong, Surface Science, 498 (2002) L103-L108.

14. S. Banerjee, J. Gopal, and P. Muraleedharan, Current Science, 90 (2006) 1378-1383.

15. J. C. Ireland, P. Klostermann, E. W. Rice, and R. M. Clark, Appl Environ Microbiol. 59 (1993) 1668-1670.

16. M. Cho, H. Chung, W. Choi, and J. Yoon, Appl Environ Microbiol. 71 (2005) 270-275.

17. H. Gerischer and A. Heller, J. Electrochem. Soc. 139 (1992) 113-118.

18. C. M. Wang, A. Heller, and H. Gerischer, J. Amer. Chem. Soc. 114 (1992) 5230-5234.

19. A. Sobczynski and A. Sobczynska, Pol. J. Appl. Chem. 40 (1996) 339-353.

20. I. Izumi, W. W. Dunn, K. O. Wilbourn, F. Fun, and A. J. Bard, J. Phys. Chem. 84 (1980) 3207-3210.

21. S. Sakaguchi, Y. Muraoka, and M. Murase, Jpn. Kokai Tokyo Koho JP, 10 (1998) 439.

22. T. Oishi, T. Ishikawa, D. Kamoto, C. Yoshioka, and O. Takahashi, Jpn. Kokai Tokyo Koho JP, 10 (1998) 597.

23. H. C. Schwarzer and W. Peukert, Chem Eng Sci. 60 (2005) 11-25.

24. R. Hunter, Foundations of Colloid Science, Oxford University Press, New York, USA, 2001.

25. H. Z. Zhang, R. L. Penn, R. J. Hamers, and J. F. Banfield, J Phys Chem B, 103 (1999) 4656-4662.

26. H. Uchida, S. Hirao, T. Torimoto, S. Kuwabata, T. Sakata, H. Mori, and H. Yoneyama, Langmuir, 11 (1995) 3725-3729.

27. Z. Zhang, C. C. Wang, R. Zakaria, and J. Y. Ying, J. Phys. Chem. B, 102 (1998) 10871-10878.

28. A. J. Maira, K. L. Yeung, C. Y. Lee, P. L. Yue, and C. K. Chan, J. Catalysis, 192 (2000) 185-196.

29. I. N. Martyanov and K. J. Klabunde, J.Catalysis, 225 (2004) 408-416.

30. S. Laachir, M. Moussetad, R. Adhiri, and A. Fahli, Electronic Journal of Theoretical Physics, 5 (2005) 12-20.

31. J. R. Harbour, V. Chow, and J. R. Bolton, Can. J. Chem. 52 (1974) 3549-3553.

32. J. R. Harbour and M. L. Hair, J. Phys. Chem. 83 (1979) 652-656.

33. J. D. Murray, Mathematical Biology I: An introduction, Springer-Verlag, New York, USA, 2002.

34. T. Ozawa, M. Iwasaki, H. Tada, T. Akita, K. Tanaka, and S. Ito, J. Colloid and Interface Sci. 281 (2005) 510-513.

35. D. C. Hurum, A. G. Agrios, K. A. Gray, T. Rajh, and M. C. Thurnauer, J. Phys. Chem. B 107 (2003) 4545-4549.

36. S. D. Mo and W. Y. Ching, Phys. Rev. B 51 (1995) 13023-13032.

37. G. M. Rosen, B. E. Britigan, H. J. Halpern, and S. Pou, in "Free radicals. Biology and detection by spin trapping" (Oxford University Press, USA, 1999)

38. A. M. Volodin, A. E. Cherkashin, and V. S. Zakharenko, React. Kinet. Catal. Lett. 11 (1979) 103-106.

39. A. M. Volodin, A. E. Cherkashin, and V. S. Zakharenko, React. Kinet. Catal. Lett., 11 (1979) 107-111.